Published in final edited form as:
Bone. 2013 January ; 52(1): 212–219. doi:10.1016/j.bone.2012.09.035.

Angiogenesis is Required for Stress Fracture Healing in Rats

Ryan E. Tomlinson[a,b], **Jennifer A. McKenzie**[a], **Anne H. Schmieder**[c], **Gregory R. Wohl**[a,1], **Gregory M. Lanza**[b,c], and **Matthew J. Silva**[a,b]

Jennifer A. McKenzie: mckenziej@wudosis.wustl.edu; Anne H. Schmieder: anne@cmrl.wustl.edu; Gregory M. Lanza: greg@cvu.wustl.edu; Matthew J. Silva: silvam@wustl.edu

[a]Department of Orthopaedic Surgery, Washington University in St. Louis, Saint Louis, MO, USA

[b]Department of Biomedical Engineering, Washington University in St. Louis, Saint Louis, MO, USA

[c]Department of Medicine, Division of Cardiology, Washington University in St. Louis, Saint Louis, MO, USA

Abstract

Although angiogenesis and osteogenesis are critically linked, the importance of angiogenesis for stress fracture healing is unknown. In this study, mechanical loading was used to create a non-displaced stress fracture in the adult rat forelimb. Fumagillin, an anti-angiogenic agent, was used as the water soluble analogue TNP-470 (25 mg/kg) as well as incorporated into lipid-encapsulated $\alpha_v\beta_3$ integrin targeted nanoparticles (0.25 mg/kg). In the first experiment, TNP-470 was administered daily for 5 days following mechanical loading, and changes in gene expression, vascularity, and woven bone formation were quantified. Although no changes in vascularity were detected 3 days after loading, treatment-related downregulation of angiogenic (*Pecam1*) and osteogenic (*Bsp*, *Osx*) genes was observed at this early time point. On day 7, microCT imaging of loaded limbs revealed diminished woven bone formation in treated limbs compared to vehicle treated limbs. In the second experiment, $\alpha_v\beta_3$ integrin targeted fumagillin nanoparticles were administered as before, albeit with a 100-fold lower dose, and changes in vascularity and woven bone formation were determined. There were no treatment-related changes in vessel count or volume 3 days after loading, although fewer angiogenic (CD105 positive) blood vessels were present in treated limbs compared to vehicle treated limbs. This result manifested on day 7 as a reduction in total vascularity, as measured by histology (vessel count) and microCT (vessel volume). Similar to the first experiment, treated limbs had diminished woven bone formation on day 7 compared to vehicle treated limbs. These results indicate that angiogenesis is required for stress fracture healing, and may have implications for inducing rapid repair of stress fractures.

Keywords

Woven bone formation; angiogenesis; TNP-470; fumagillin; mechanical loading; stress fracture

Corresponding Author: Ryan E. Tomlinson, 425 S. Euclid Avenue, Campus Box 8233, St. Louis MO 63110, + 1-314-747-6070 (phone), + 1-314-362-0334 (fax), ryan.tomlinson@wustl.edu.
[1]Present address: Department of Mechanical Engineering, McMaster University, Hamilton ON, Canada, wohlg@mcmaster.ca

1. INTRODUCTION

Osteogenesis, the process of new bone tissue formation, is strongly related to angiogenesis, the process by which new vessels extend from the existing vascular system [1]. In fact, it has been shown that many osteogenic processes, including fracture healing [1, 2], distraction osteogenesis [3–5], skeletal development [6], and others [7, 8] are critically dependent on angiogenesis. Repetitive mechanical loading of the skeleton also stimulates osteogenesis, but the role of angiogenesis in this context is not well understood.

In general, mechanical loading at hyperphysiological strain levels leads to the formation of woven bone rather than lamellar bone [9]. In the rat forelimb, a single bout of damaging, cyclic loading has been shown to reproducibly generate a non-displaced stress fracture that leads to woven bone formation at the ulnar mid-diaphysis [10, 11]. In this scenario, woven bone formation is associated with the upregulation of angiogenic genes (*Vegf*, *Pecam1*) and increased vascularity [12–14]. In addition, blood flow rate is increased at the site of woven bone formation 1 week after mechanical loading [15]. These results suggest that angiogenesis may be a requirement for the woven bone formation response after a stress fracture.

Fumagillin, a hydrophobic mycotoxin produced by Aspergillus fumagatus, and TNP-470, a water soluble semisynthetic derivative of fumagillin, suppress angiogenesis by inhibition of methionine aminopeptidase 2 [16]. In preclinical tumor models, TNP-470 has been shown to inhibit cancer growth and bone metastasis [17–19]. In addition, TNP-470 has been shown to prevent fracture healing [2] and bone formation during distraction osteogenesis [3] in animal studies. However, therapeutic systemic dosages of this drug can cause neurotoxicity [20, 21]. Targeted nanoparticle delivery permits lower overall dosages to be effective at specific sites of interest [22]. The $\alpha_v\beta_3$ integrin has been shown to be a marker for blood vessels undergoing angiogenesis [23, 24], and its expression diminishes as blood vessels mature [25]. Thus, by targeting the $\alpha_v\beta_3$ integrin, only neovasculature is affected whereas quiescent (mature) vessels are not. Recently, $\alpha_v\beta_3$ integrin targeted fumagillin nanoparticles have been shown to effectively inhibit blood vessel formation in tumors and atherosclerosis [22, 26–29].

The objective of this study was to determine if anti-angiogenic treatment affects stress fracture healing. To uncover the relationship of angiogenesis to osteogenesis in this process, changes in gene expression, woven bone formation, and vascularity were measured after damaging osteogenic mechanical loading in adult rats with and without anti-angiogenic treatment.

2. METHODS & MATERIALS

2.1 Mechanical Loading

Male Fischer (F344/NHsd) rats were obtained at 13–14 weeks of age (Harlan) and housed under standard conditions until 18–22 weeks of age. The right forelimb of each rat was mechanically loaded using an established stress fracture (fatigue) protocol [10] known to stimulate an abundant woven bone formation response at the mid-diaphysis of the ulna. First, rats were anesthetized with isoflurane gas (1–3%). The right forelimb was axially compressed by placing the olecranon process and the flexed carpus into specially designed fixtures. A material testing system (Instron Electropuls 1000 or Dynamite 8841) was used to apply force and monitor displacement. A 0.3 N compressive pre-load was applied followed by a cyclic haversine waveform of 18 N at 2 Hz until an increase in peak displacement equal to 65% of the displacement to fracture (1.3 mm, relative to the 10th cycle) was achieved [12, 30]. The left forelimb was not mechanically loaded, and was used as an internal control.

Following the procedure, rats were given an intramuscular injection of analgesic (0.05 mg/kg buprenorphine) and allowed unrestricted cage activity. Animals were euthanized by CO_2 asphyxiation unless otherwise noted. All protocols were approved by our institution's Animal Studies Committee.

2.2 TNP-470

In the first round of investigation, TNP-470 (25 mg/kg s.c.; a gift from Takeda Pharmaceutical), an agent known to inhibit angiogenesis [16, 17], or vehicle (40% (v/v) ethanol in phosphate buffered saline (PBS)), was administered daily for up to 5 days; the first injection was 1 hour prior to loading. Animals were euthanized 1 hour, 1 day, or 3 days after loading for gene expression analysis (n = 6 per group), 3 days after loading for vascular perfusion (n = 6 per group), and 7 days after loading for analysis of bone formation using microCT and dynamic histomorphometry (n = 6 per group).

2.3 $\alpha_v\beta_3$ targeted fumagillin nanoparticles

In the second round of investigation, lipid-encapsulated $\alpha_v\beta_3$ integrin targeted fumagillin nanoparticles were used to inhibit angiogenesis. After loading, each rat was given a daily injection of nanoparticles (0.25 mg/kg i.v.) or vehicle (sterile water) for up to 5 days; the first injection was 1 hour prior to loading. The nanoparticles were directed to the $\alpha_v\beta_3$ integrin with a peptidomimetic vitronectin antagonist developed by Bristol-Myers Squibb Medical Imaging (U.S. patent 6,511,648 and related patents), as described previously [22]. In general, nanoparticles were comprised of 20% (v/v) perfluorooctylbromide (Exfluor Research Corporation) and 2.0% (w/v) of a surfactant co-mixture, 1.7% (w/v) glycerin, and water for the balance. The surfactant commixture included 99 mol% highly purified egg yolk lecithin (Avanti Polar Lipids), and 0.1 mg/mL of the $\alpha_v\beta_3$ integrin antagonist conjugated to PEG2000-phosphatidylethanolamine (Kereos, Inc.). The surfactant components were dissolved in chloroform/methanol and dried in a 50 °C vacuum oven overnight. Nanoparticles were modified to include 0.1 mg/mL fumagillin (a gift from the National Cancer Institute) and 0.1 mg/mL Alexafluor594 (conjugated to lipid), which were substituted to the surfactant mixture at the expense of lecithin on an equimolar basis. Animals were euthanized 3 and 7 days after loading for vascular perfusion and immunohistochemistry (n = 7 or more per group), and 7 days after loading to assess bone formation using microCT imaging (n = 7 per group).

2.4 Gene Expression

Changes in gene expression were assessed in treated and vehicle animals using quantitative real time PCR (qPCR) with established methods [14]. Briefly, right and left ulnae (with surrounding periosteal tissue intact) were dissected and immediately placed into liquid nitrogen. A 5 mm section from the central ulna was pulverized, suspended in TRIzol (Invitrogen) and RNA extracted (Qiagen). RNA quantity (Nanodrop; 260/280 ratio average 2.01) and quality (Agilent bioanalyzer; RIN average 7.97) were assessed before making 1 μg cDNA (Superscript III, Invitrogen). qPCR was run (Applied Biosystems 7300) using validated primers [14] and Sybr® Green based detection. Five genes were evaluated, including the angiogenic markers vascular endothelial growth factor (*Vegf*) and platelet endothelial cell adhesion molecular (*Pecam1*), as well as the osteogenic markers bone morphogenetic protein 2 (*Bmp2*), osterix (*Osx*) and bone sialoprotein (*Bsp*). Measures of real-time PCR cycle to threshold were normalized to the expression of reference gene glyceraldehyde-3-phosphate dehydrogenase (*Gapdh*) for each ulna. To obtain a fold change comparison between experimental groups, *Gapdh*-normalized expression from each loaded ulna was divided by the normalized gene expression from the non-loaded contralateral control ($2_{-\Delta\Delta Ct}$).

2.5 Vascular Perfusion

Vessel morphology was quantified using an established vascular perfusion technique [13, 31]. Animals were anesthetized using isoflurane gas (1–3%). After median sternotomy, an 18 gauge catheter was inserted into the aorta through the left ventricle and secured using adhesive (Loctite® 4471™, Henkel Technologies). After injection of 10 mL of Heparin Lock Flush (100 U/mL) to inhibit clotting, the animal was euthanized by exsanguination. The vasculature was then irrigated with approximately 100 mL of PBS at 37 °C. Finally, 60 mL of silicone rubber (Microfil® MV-122, Flow Tech Inc.) was injected and allowed to cure overnight at 4 °C. After curing, the forelimb was harvested and fixed in 10% buffered formalin (Fisher Scientific) for 16–24 hours. After imaging (see: MicroCT Imaging), forelimbs were decalcified (14% EDTA) and embedded in paraffin. Transverse 5 μm sections were cut 1 mm distal to the midpoint (site of maximal bone formation [10]) and stained with hematoxylin and eosin. Digital images of these sections were captured using bright field microscopy (Olympus BX-51) with a 10X objective. Perfused vessels in the expanded periosteum were segmented from surrounding tissue using a color threshold in Adobe Photoshop (Adobe Systems, Inc.). Using the segmented images, vessel count was calculated using ImageJ (NIH). Vessels were counted in the expanded periosteum, defined as the tissue located between the original cortical surface of the bone and the adjacent muscle.

2.6 Dynamic Histomorphometry

Rats were given intraperitoneal injections of fluorescent bone formation markers immediately after loading (calcein green - 5 mg/kg, Sigma) and 5 days after loading (alizarin complexone - 30 mg/kg, Sigma). Two days later, forelimbs were harvested and fixed as above. After imaging (see: MicroCT Imaging), forelimbs were embedded in poly-(methyl methacrylate). Transverse thick sections were cut (SP 1600, Leica Microsystems) 1 mm distal to the midpoint, then polished to 100 μm and mounted on glass slides. Digital images of these sections were captured using fluorescence microscopy (Olympus IX-51) with fluorescein isothiocyanate (FITC) and tetramethylrhodamine isothiocyanate (TRITC) filters for calcein and alizarin, respectively. Images were analyzed in Bioquant for woven bone area.

2.7 MicroCT Imaging

Ex vivo micro computed tomography (μCT40, Scanco Medical AG) was used to analyze bone formation at the ulnar mid-diaphysis 7 days after mechanical loading. The central 8 mm of each ulna was scanned separately (45 kV, 177 μA, medium resolution, 200 msec integration, 16 μm voxel size). Scan slices were in the transverse plane (the forelimb was placed parallel to the z-axis of the scanner). Hand drawn contours (sigma = 1.2, support = 2, lower/upper threshold = 275/1000) were used to manually segment volumes of Microfil-perfused vessels (if applicable), newly formed woven bone, and original cortical bone using Scanco imaging software. In addition, the axial length along which new woven bone had formed (woven bone extent) was measured for each sample.

2.8 Immunohistochemistry

To evaluate the vasculature in the expanded periosteum at the ulnar mid-diaphysis using immunohistochemistry, transverse 5 μm sections of formalin-fixed, paraffin-embedded forelimbs were cut 1 mm distal to the midpoint. After deparaffination in xylene and rehydration in graded ethanol solutions, antigen retrieval was performed with either 2.1% boric acid at 55 °C overnight (CD105) or by microwaving slides in 0.01 M citrate buffer twice for 4 minutes (αSMA). Fifteen minute incubation in 3% H_2O_2 was used to block endogenous peroxidase activity, and sections were incubated in Ultra V Block (Thermo

Scientific) to reduce nonspecific background staining. Following this, rabbit polyclonal CD105 antibody (sc-20632, Santa Cruz – 1:400 dilution) or mouse monoclonal anti-α-smooth muscle actin (A2547, Sigma – 1:1000 dilution) was applied using Ultra Clean Antibody Diluent (Thermo Scientific) at 4 °C overnight. Negative control slides were prepared by substituting normal goat serum for the primary antibody. To visualize binding, biotinylated goat anti-polyvalent (Thermo Scientific) was applied for 15 minutes followed by streptavidin peroxidase (Thermo Scientific) for 15 minutes and 1:4 dilution of VIP (Vector) for 10 minutes. The slides were then dehydrated, mounted, and examined with bright field microscopy. Positively stained vessels were counted in the expanded periosteum, defined as the tissue located between the original cortical surface of the bone and the adjacent muscle.

2.9 Statistics

Data from the two rounds of experimentation were analyzed separately. Two-way analysis of variance (ANOVA) was used to compare across treatment groups and time points. Differences between individual treatment groups and time points were assessed using Fisher's protected least significant difference test, while differences between loaded and non-loaded limbs were assessed using paired t-tests. In each case, $p < 0.05$ was considered significant.

3. RESULTS

3.1 TNP-470

In the first round of investigation, TNP-470 was used to inhibit angiogenesis following a stress fracture induced by mechanical loading. Both angiogenic (*Vegf*, *Pecam1*) and osteogenic (*Bmp2*, *Osx*, *Bsp*) genes were considered 1 hour, 1 day, and 3 days after loading for animals treated with TNP-470 and vehicle (Fig. 1). At 1 hour after loading, *Bmp2, Pecam1* and *Vegf* were significantly upregulated in both TNP-470 and vehicle treated limbs compared to non-loaded limbs. Moreover, at 1 day and 3 days after loading, all five genes were significantly upregulated in both TNP-470 and vehicle treated loaded limbs compared to non-loaded limbs. However, in TNP-470 treated limbs the upregulation of *Bsp*, *Osx*, and *Pecam1* was significantly less compared to vehicle treated limbs 3 days after loading, illustrating differential gene expression due to anti-angiogenic treatment.

Vasculature was perfused 3 days after loading and quantified using histology and microCT. Regardless of treatment, there were significant increases in vessel count and volume in loaded limbs compared to non-loaded limbs. Contrary to our expectation, treatment with TNP-470 did not decrease vascularity in loaded limbs compared to vehicle treatment by day 3 (*not shown*).

Bone formation was quantified using microCT and dynamic histomorphometry at day 7 (Fig. 2). Woven bone was evident in loaded limbs but absent in non-loaded limbs. In contrast to vascularity, woven bone extent (− 30%) and woven bone area (−60%) were significantly less in TNP-470 treated limbs compared to vehicle treated limbs. Because treatment-related reductions in bone formation and osteogenic and angiogenic gene expression were observed without measurable changes in vascularity at day 3, a second round of investigation was initiated with an additional vascular time point at day 7 and new outcome measurements.

3.2 $\alpha_v\beta_3$ targeted fumagillin nanoparticles

In the second round of investigation, $\alpha_v\beta_3$ integrin targeted fumagillin nanoparticles were used to inhibit angiogenesis after osteogenic mechanical loading. Vasculature was perfused

3 and 7 days after loading and quantified using histology and microCT. Similar to treatment with TNP-470, nanoparticle treatment did not result in significant differences in vessel count or volume compared to vehicle treatment when evaluated 3 days after loading. However, 7 days after loading, nanoparticle treatment resulted in dramatic changes in vascularity with significantly fewer vessels (−30%) and significantly less vessel volume (−33%) compared to vehicle treatment (Fig. 3).

Bone formation was quantified using microCT imaging on day 7. Similar to TNP-470 treatment, treatment with fumagillin nanoparticles resulted in diminished bone formation, with significantly decreased woven bone extent (−30%) and less woven bone volume (−25%) in nanoparticle treated limbs compared to vehicle treated limbs (Fig. 4).

Immunohistochemistry was used to further assess vasculature by counting blood vessels stained positive for CD105 (a marker for angiogenic vessels) and αSMA (a marker for mature vessels). Loaded limbs had significantly more CD105 positive vessels than non-loaded limbs at day 3 (Fig. 5B). However, loaded limbs had significantly fewer (−50%) CD105 positive vessels in nanoparticle treated animals compared to vehicle treated animals at day 3. Similarly, loaded limbs had significantly more αSMA positive vessels than non-loaded limbs at day 7 (Fig. 5D). However, loaded limbs from nanoparticle treated animals had significantly fewer (−25%) αSMA positive vessels compared to vehicle at day 7. Thus, anti-angiogenic treatment resulted in fewer angiogenic vessels at day 3 which led to fewer mature vessels by day 7.

4. DISCUSSION

The goal of this study was to examine the effects of inhibiting angiogenesis after a non-displaced stress fracture generated by damaging mechanical loading. Two treatments were used to inhibit angiogenesis: TNP-470 and $\alpha_v\beta_3$ integrin targeted fumagillin nanoparticles. The results from vascular perfusion, microCT, dynamic histomorphometry, immunohistochemistry, and gene expression illustrate that anti-angiogenic treatment decreases vascularity, woven bone formation, and osteogenic and angiogenic gene expression at the site of stress fracture repair.

This study provides new insight into the timing of vascular changes during skeletal repair after a stress fracture from repetitive mechanical loading. A large increase in CD105 positive blood vessels was observed near the site of woven bone formation 3 days after loading. Because CD105 is a marker predominantly expressed in angiogenic endothelial cells [32], an increase in CD105 positive vessels should immediately precede an increase in vascularity. Indeed, vessel volume increased significantly in loaded limbs between days 3 and 7. Anti-angiogenic treatment almost completely blunted the loading-induced increase in angiogenic (CD105 positive) vessels on day 3, and subsequently diminished the number of mature (αSMA positive) vessels as well as the total vasculature (vessel count and volume) in loaded limbs on day 7. Since anti-angiogenic treatment does not result in significant differences in vascularity by day 3, our data indicate that limited angiogenesis occurs in the first 72 hours after loading. The gene expression data support this timeline. There were no treatment-related differences in gene expression in the first 24 hours after loading. However, *Pecam1*, *Osx*, and *Bsp* were significantly decreased in TNP-470 treated limbs on day 3, suggesting that anti-angiogenic treatment impaired angiogenic sprouting as well as bone formation capacity by day 3. These results indicate that significant vascular expansion from angiogenesis starts approximately 3 days after stress fracture.

The upregulation of angiogenic genes (*Vegf*, *Pecam1*) has been shown to immediately follow a stress fracture generated by damaging mechanical loading [14], and apparent

vascularity is significantly greater in loaded limbs compared to non-loaded limbs 3 days after loading [12, 13]. Although the increase in apparent vascularity was originally taken as evidence of early angiogenesis, this study taken together with the previous data has lead to the hypothesis that the early response to damaging mechanical loading is the opening of dynamic vessel networks and marked vasodilation. These processes are independent from angiogenesis, which has been shown here to occur later, likely in response to the metabolic demand of increased bone mass. The process of inducing rapid patency of dormant vessels has been observed previously in studies of intrapulmonary arteriovenous anastomoses in humans and dogs [33, 34]. Although the exact mechanism for this phenomenon is not well understood, hypoxia may play a major role [35]. In previous studies of stress fracture repair, hypoxia inducible factor 1α (*Hif1a*) was shown to be significantly increased as early as 1 hour after loading, and this significant increase persisted as long as 11 days after loading [12, 36]. These data indicate that the immediate response to a stress fracture generated by damaging mechanical loading is a local hypoxic environment, consistent with the proposed mechanism for rapidly opening dynamic vessel networks. However, *Hif1a* has also been shown to be regulated by mechanical stress [37–40], so more research is required to better understand this process, particularly in the context of loading-induced woven bone formation.

In this study, data from two angiogenic inhibition experiments was presented, one using TNP-470 and the other using $\alpha_v\beta_3$ integrin targeted fumagillin nanoparticles. Although these two anti-angiogenic treatments act through the same mechanism (methionine aminopeptidase 2 inhibition [16]), the compound is not identical (TNP-470 vs. fumagillin) and the dosage differs by two orders of magnitude (25 mg/kg vs. 0.25 mg/kg). Since $\alpha_v\beta_3$ antagonists alone have been shown to inhibit angiogenesis [23, 25], the $\alpha_v\beta_3$ integrin targeted nanoparticles may be preventing angiogenesis independent of fumagillin. Although the $\alpha_v\beta_3$ integrin is also essential for osteoclast function [41], the nanoparticles are constrained to the vascular system due to their size [42]. The water soluble TNP-470 may be able to affect targets outside the blood supply, and has been shown to inhibit osteoclast resorption *in vitro* [19]. However, osteoclasts do not appear in detectable numbers until the second week after stress fracture in this model [43, 44], so osteoclast-related effects are unlikely to have played a role in this study. Nonetheless, the lower drug dosage, additional mechanism of action, and vascular specificity make targeted nanoparticles preferable for future experimentation.

In previous studies, TNP-470 (30 mg/kg) completely prevented endochondral bone healing after closed femoral fracture in rats [2], as well as intramembranous bone formation occurring during gradual distraction osteogenesis [3]. However, in the current study, angiogenic inhibition using either TNP-470 or targeted nanoparticles diminishes, but does not completely prevent, woven bone formation. The amount of woven bone formed after angiogenic inhibition was similar to the amount formed from less severe stress fractures (displacement in the range of 30% to 45% of fracture [10], rather than the 65% displacement used here). Although treatment likely did not completely eliminate angiogenic sprouting in the region of interest, the existing vascular system may have been able to support a limited amount of woven bone formation despite inhibited angiogenesis. This phenomenon has been indirectly observed in previous work, where no significant changes in vessel count were found despite limited woven bone formation occurring after 30% displacement to fracture [13]. Therefore, these data suggest that angiogenesis is a response to the increased metabolic demand of newly formed woven bone, but may not be required for the initiation of woven bone formation. Additionally, the amount of angiogenesis driven by loading may have been underestimated in this model, since only periosteal vasculature was quantified. It is possible that intramedullary and intracortical angiogenesis may also be occurring, although given the small medullary cavity at the site of interest as well as the relatively early time points of this

study (prior to intracortical resorption), any contribution from these sources is negligible. Nonetheless, these results clearly indicate that angiogenesis is necessary for a full osteogenic response to a stress fracture generated by damaging mechanical loading. Finally, the results of this study suggest that stress fracture healing could be accelerated by increasing vascular capacity or angiogenicity at the site of skeletal repair.

5. CONCLUSION

In summary, TNP-470 and $\alpha_v\beta_3$ targeted fumagillin nanoparticles were used to inhibit angiogenesis after a forelimb stress fracture from damaging mechanical loading in rats. There were no changes in vascularity 3 days after loading, but fewer angiogenic (CD105 positive) blood vessels were present at the site of bone formation in treated animals. Three days after loading, angiogenic (*Pecam1*) and osteogenic (*Bsp*, *Osx*) genes were less upregulated in treated limbs than vehicle limbs. Seven days after loading, treatment was associated with less vasculature (blood vessel count and volume) and less woven bone (woven bone extent, area, and volume). Taken together, these results demonstrate that vascular expansion by angiogenesis begins about 3 days after a stress fracture and is required for a full osteogenic response.

Acknowledgments

This study was funded by a grant from the National Institutes of Health (NIH R01 AR050211) and was performed at a facility supported by the Washington University Musculoskeletal Research Center (NIH P30 AR057235). In addition, we acknowledge additional nanomedicine research support from the NIH (HL113392, CA100623, CA154737, HL094470, AR056468, NS073457, CA136398) and the American Heart Association (0835426N and 11IRG5690011). Dr. Lanza is a scientific cofounder of Kereos, Inc, St. Louis, which has licensed angiogenesis-targeted perfluorocarbon nanotechnology intellectual property from Washington University/Barnes-Jewish Hospital for clinical development. The authors would like to thank Dr. Huiying Zhang for her assistance with immunohistochemistry and Ralph W. Fuhrhop for preparation of the nanoparticle formulations.

References

1. Glowacki J. Angiogenesis in fracture repair. Clinical Orthopaedics and Related Research. 1998 Oct.:S82–S89. [PubMed: 9917629]
2. Hausman MR, Schaffler MB, Majeska RJ. Prevention of fracture healing in rats by an inhibitor of angiogenesis. Bone. 2001; 29:560–564. [PubMed: 11728927]
3. Fang TD, Salim A, Xia W, Nacamuli RP, Guccione S, Song HM, Carano RA, Filvaroff EH, Bednarski MD, Giaccia AJ, Longaker MT. Angiogenesis is required for successful bone induction during distraction osteogenesis. Journal of Bone and Mineral Research. 2005; 20:1114–1124. [PubMed: 15940364]
4. Jazrawi LM, Majeska RJ, Klein ML, Kagel E, Stromberg L, Einhorn TA. Bone and cartilage formation in an experimental model of distraction osteogenesis. Journal of Orthopaedic Trauma. 1998; 12:111–116. [PubMed: 9503300]
5. Li G, Simpson AH, Kenwright J, Triffitt JT. Effect of lengthening rate on angiogenesis during distraction osteogenesis. Journal of Orthopaedic Research. 1999; 17:362–367. [PubMed: 10376724]
6. Pechak DG, Kujawa MJ, Caplan AI. Morphological and histochemical events during first bone formation in embryonic chick limbs. Bone. 1986; 7:441–458. [PubMed: 3541986]
7. Leunig M, Yuan F, Gerweck LE, Jain RK. Effect of basic fibroblast growth factor on angiogenesis and growth of isografted bone: quantitative in vitro-in vivo analysis in mice. International Journal of Microcirculation. 1997; 17:1–9.
8. Winet H, Hollinger JO, Stevanovic M. Incorporation of polylactide-polyglycolide in a cortical defect: neoangiogenesis and blood supply in a bone chamber. Journal of Orthopaedic Research. 1995; 13:679–689. [PubMed: 7472746]
9. Frost HM. From Wolff's law to the Utah paradigm: insights about bone physiology and its clinical applications. The Anatomical Record. 2001; 262:398–419. [PubMed: 11275971]

10. Uthgenannt BA, Kramer MH, Hwu JA, Wopenka B, Silva MJ. Skeletal self-repair: stress fracture healing by rapid formation and densification of woven bone. Journal of Bone and Mineral Research. 2007; 22:1548–1556. [PubMed: 17576168]
11. Torrance AG, Mosley JR, Suswillo RF, Lanyon LE. Noninvasive loading of the rat ulna in vivo induces a strain-related modeling response uncomplicated by trauma or periostal pressure. Calcified Tissue International. 1994; 54:241–247. [PubMed: 8055374]
12. McKenzie JA, Silva MJ. Comparing histological, vascular and molecular responses associated with woven and lamellar bone formation induced by mechanical loading in the rat ulna. Bone. 2011; 48:250–258. [PubMed: 20849995]
13. Matsuzaki H, Wohl GR, Novack DV, Lynch JA, Silva MJ. Damaging fatigue loading stimulates increases in periosteal vascularity at sites of bone formation in the rat ulna. Calcified Tissue International. 2007; 80:391–399. [PubMed: 17551770]
14. Wohl GR, Towler DA, Silva MJ. Stress fracture healing: fatigue loading of the rat ulna induces upregulation in expression of osteogenic and angiogenic genes that mimic the intramembranous portion of fracture repair. Bone. 2009; 44:320–330. [PubMed: 18950737]
15. Tomlinson RE, Silva MJ, Shoghi KI. Quantification of skeletal blood flow and fluoride metabolism in rats using PET in a pre-clinical stress fracture model. Molecular Imaging and Biology. 2012; 14:348–354. [PubMed: 21785919]
16. Sin N, Meng L, Wang MQ, Wen JJ, Bornmann WG, Crews CM. The anti-angiogenic agent fumagillin covalently binds and inhibits the methionine aminopeptidase, MetAP-2. Proceedings of the National Academy of Sciences of the United States of America. 1997; 94:6099–6103. [PubMed: 9177176]
17. Kruger EA, Figg WD. TNP-470: an angiogenesis inhibitor in clinical development for cancer. Expert Opinion on Investigational Drugs. 2000; 9:1383–1396. [PubMed: 11060750]
18. Singh Y, Shikata N, Kiyozuka Y, Nambu H, Morimoto J, Kurebayashi J, Hioki K, Tsubura A. Inhibition of tumor growth and metastasis by angiogenesis inhibitor TNP-470 on breast cancer cell lines in vitro and in vivo. Breast Cancer Research and Treatment. 1997; 45:15–27. [PubMed: 9285113]
19. Sasaki A, Alcalde RE, Nishiyama A, Lim DD, Mese H, Akedo H, Matsumura T. Angiogenesis inhibitor TNP-470 inhibits human breast cancer osteolytic bone metastasis in nude mice through the reduction of bone resorption. Cancer Research. 1998; 58:462–467. [PubMed: 9458090]
20. Bhargava P, Marshall JL, Rizvi N, Dahut W, Yoe J, Figuera M, Phipps K, Ong VS, Kato A, Hawkins MJ. A Phase I and pharmacokinetic study of TNP-470 administered weekly to patients with advanced cancer. Clinical Cancer Research. 1999; 5:1989–1995. [PubMed: 10473076]
21. Kudelka AP, Verschraegen CF, Loyer E. Complete remission of metastatic cervical cancer with the angiogenesis inhibitor TNP-470. The New England Journal of Medicine. 1998; 338:991–992. [PubMed: 9527612]
22. Wickline SA, Neubauer AM, Winter P, Caruthers S, Lanza G. Applications of nanotechnology to atherosclerosis, thrombosis, and vascular biology. Arteriosclerosis, Thrombosis, and Vascular Biology. 2006; 26:435–441.
23. Brooks PC, Clark RA, Cheresh DA. Requirement of vascular integrin alpha v beta 3 for angiogenesis. Science. 1994; 264:569–571. [PubMed: 7512751]
24. Brooks PC, Montgomery AM, Rosenfeld M, Reisfeld RA, Hu T, Klier G, Cheresh DA. Integrin alpha v beta 3 antagonists promote tumor regression by inducing apoptosis of angiogenic blood vessels. Cell. 1994; 79:1157–1164. [PubMed: 7528107]
25. Storgard CM, Stupack DG, Jonczyk A, Goodman SL, Fox RI, Cheresh DA. Decreased angiogenesis and arthritic disease in rabbits treated with an alphavbeta3 antagonist. The Journal of Clinical Investigation. 1999; 103:47–54. [PubMed: 9884333]
26. Winter PM, Caruthers SD, Zhang H, Williams TA, Wickline SA, Lanza GM. Antiangiogenic synergism of integrin-targeted fumagillin nanoparticles and atorvastatin in atherosclerosis. JACC: Cardiovascular Imaging. 2008; 1:624–634. [PubMed: 19356492]
27. Winter PM, Morawski AM, Caruthers SD, Fuhrhop RW, Zhang H, Williams TA, Allen JS, Lacy EK, Robertson JD, Lanza GM, Wickline SA. Molecular imaging of angiogenesis in early-stage

atherosclerosis with alpha(v)beta3-integrin-targeted nanoparticles. Circulation. 2003; 108:2270–2274. [PubMed: 14557370]

28. Winter PM, Neubauer AM, Caruthers SD, Harris TD, Robertson JD, Williams TA, Schmieder AH, Hu G, Allen JS, Lacy EK, Zhang H, Wickline SA, Lanza GM. Endothelial alpha(v)beta3 integrin-targeted fumagillin nanoparticles inhibit angiogenesis in atherosclerosis. Arteriosclerosis, Thrombosis, and Vascular Biology. 2006; 26:2103–2109.
29. Winter PM, Schmieder AH, Caruthers SD, Keene JL, Zhang H, Wickline SA, Lanza GM. Minute dosages of alpha(nu)beta3-targeted fumagillin nanoparticles impair Vx-2 tumor angiogenesis and development in rabbits. The FASEB Journal. 2008; 22:2758–2767.
30. Uthgenannt BA, Silva MJ. Use of the rat forelimb compression model to create discrete levels of bone damage in vivo. Journal of Biomechanics. 2007; 40:317–324. [PubMed: 16519891]
31. Duvall CL, Taylor WR, Weiss D, Guldberg RE. Quantitative microcomputed tomography analysis of collateral vessel development after ischemic injury. American Journal of Physiology - Heart and Circulatory Physiology. 2004; 287:H302–H310. [PubMed: 15016633]
32. Duff SE, Li C, Garland JM, Kumar S. CD105 is important for angiogenesis: evidence and potential applications. The FASEB Journal. 2003; 17:984–992.
33. Eldridge MW, Dempsey JA, Haverkamp HC, Lovering AT, Hokanson JS. Exercise-induced intrapulmonary arteriovenous shunting in healthy humans. Journal of Applied Physiology. 2004; 97:797–805. [PubMed: 15107409]
34. Stickland MK, Lovering AT, Eldridge MW. Exercise-induced arteriovenous intrapulmonary shunting in dogs. American Journal of Respiratory and Critical Care Medicine. 2007; 176:300–305. [PubMed: 17478619]
35. Lovering AT, Elliott JE, Beasley KM, Laurie SS. Pulmonary pathways and mechanisms regulating transpulmonary shunting into the general circulation: an update. Injury. 2010; 41(Suppl 2):S16–S23. [PubMed: 21144922]
36. Martinez MD, Schmid GJ, McKenzie JA, Ornitz DM, Silva MJ. Healing of non-displaced fractures produced by fatigue loading of the mouse ulna. Bone. 2010; 46:1604–1612. [PubMed: 20215063]
37. Chang H, Shyu KG, Wang BW, Kuan P. Regulation of hypoxia-inducible factor-1alpha by cyclical mechanical stretch in rat vascular smooth muscle cells. Clinical Science. 2003; 105:447–456. [PubMed: 12780343]
38. Kim CH, Cho YS, Chun YS, Park JW, Kim MS. Early expression of myocardial HIF-1alpha in response to mechanical stresses: regulation by stretch-activated channels and the phosphatidylinositol 3-kinase signaling pathway. Circulation Research. 2002; 90:E25–E33. [PubMed: 11834720]
39. Chun YS, Kim MS, Park JW. Oxygen-dependent and -independent regulation of HIF-1alpha. Journal of Korean Medical Science. 2002; 17:581–588. [PubMed: 12378005]
40. Milkiewicz M, Doyle JL, Fudalewski T, Ispanovic E, Aghasi M, Haas TL. HIF-1alpha and HIF-2alpha play a central role in stretch-induced but not shear-stress-induced angiogenesis in rat skeletal muscle. The Journal of Physiology. 2007; 583:753–766. [PubMed: 17627993]
41. Nakamura I, Duong le T, Rodan SB, Rodan GA. Involvement of alpha(v)beta3 integrins in osteoclast function. Journal of Bone and Mineral Metabolism. 2007; 25:337–344. [PubMed: 17968485]
42. Pan D, Pramanik M, Senpan A, Allen JS, Zhang H, Wickline SA, Wang LV, Lanza GM. Molecular photoacoustic imaging of angiogenesis with integrin-targeted gold nanobeacons. The FASEB Journal. 2011; 25:875–882.
43. Hsieh YF, Silva MJ. In vivo fatigue loading of the rat ulna induces both bone formation and resorption and leads to time-related changes in bone mechanical properties and density. Journal of Orthopaedic Research. 2002; 20:764–771. [PubMed: 12168665]
44. Kidd LJ, Stephens AS, Kuliwaba JS, Fazzalari NL, Wu AC, Forwood MR. Temporal pattern of gene expression and histology of stress fracture healing. Bone. 2010; 46:369–378. [PubMed: 19836476]

Highlights

- Angiogenesis was inhibited using TNP-470 and $\alpha_v\beta_3$ integrin targeted nanoparticles.
- Treatment was associated with less vascularity and bone formation 7 days after loading.
- Angiogenesis is required for stress fracture healing in rats.

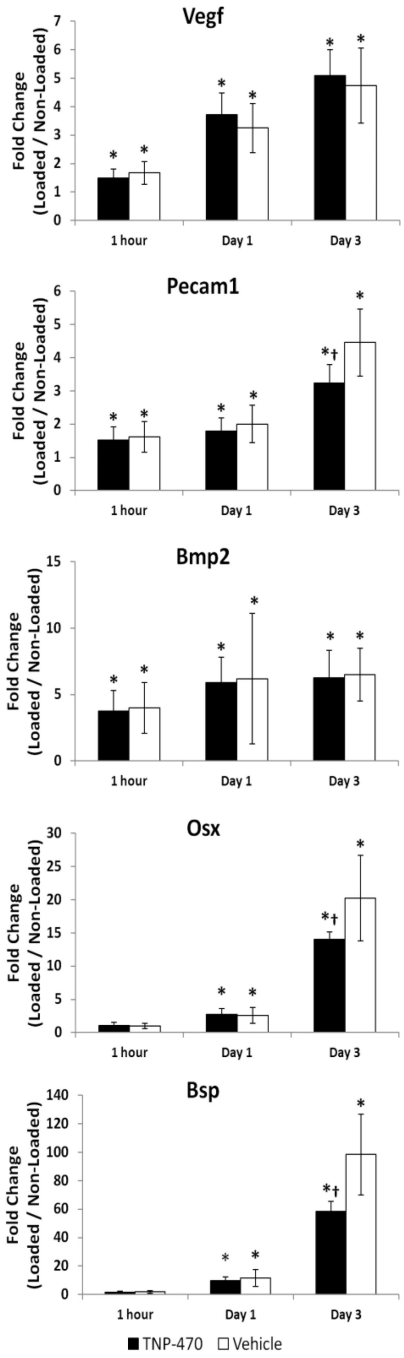

Fig. 1. Increases in Osteogenic and Angiogenic Gene Expression after Stress Fracture are Impaired by Anti-angiogenic Treatment

Genes were quantified 1 hour, 1 day, and 3 days after a stress fracture created by damaging mechanical loading. * $p < 0.05$ vs. Non-Loaded, † $p < 0.05$ vs. Vehicle.

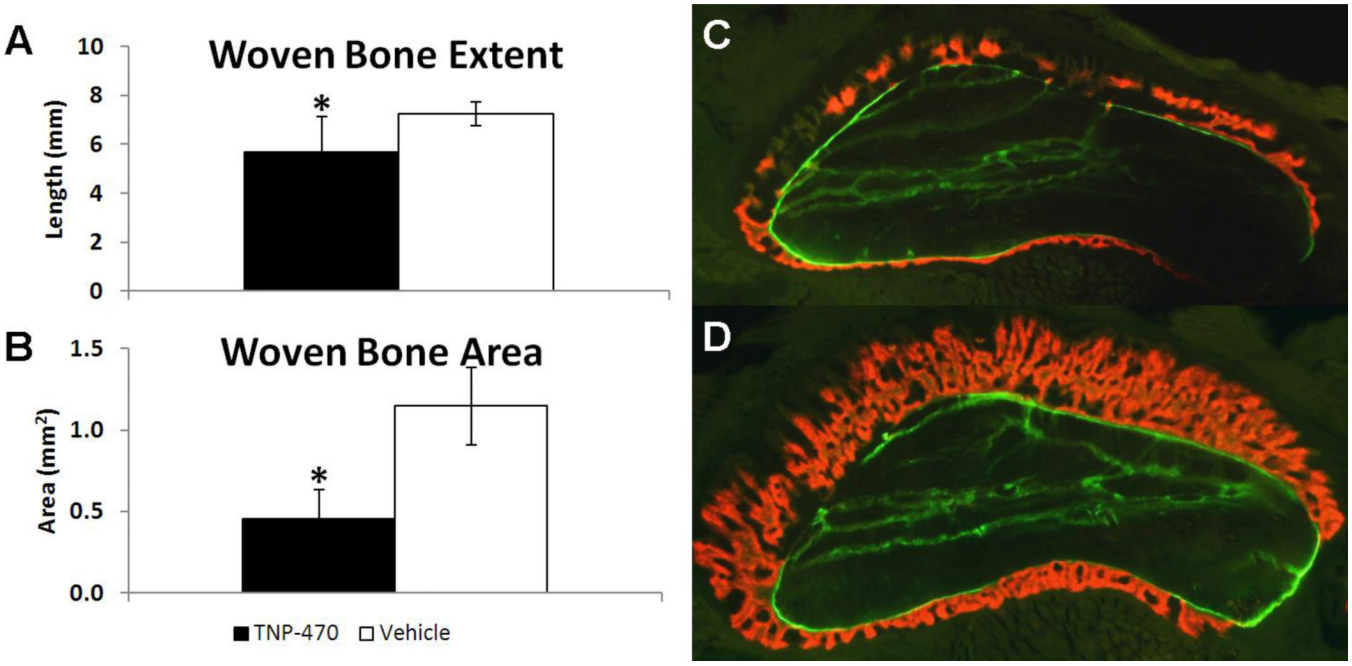

Fig. 2. Anti-angiogenic Treatment with TNP-470 Reduced Woven Bone Formation 7 days after Loading

Woven bone formation after mechanical loading and treatment with TNP-470 (black) or vehicle (white) are given as mean ± standard deviation. TNP-470 treated limbs had significantly less woven bone formation demonstrated by (A) woven bone extent measured by microCT and (B) woven bone area measured by dynamic histomorphometry. Representative cross-sectional images of ulnae with two fluorescent bone formation labels from animals treated with (C) TNP-470 or (D) vehicle illustrate the significant difference in woven bone area. Calcein (green) was given immediately after loading, followed by alizarin complexone (red) 5 days after loading. * $p < 0.05$ vs. Vehicle.

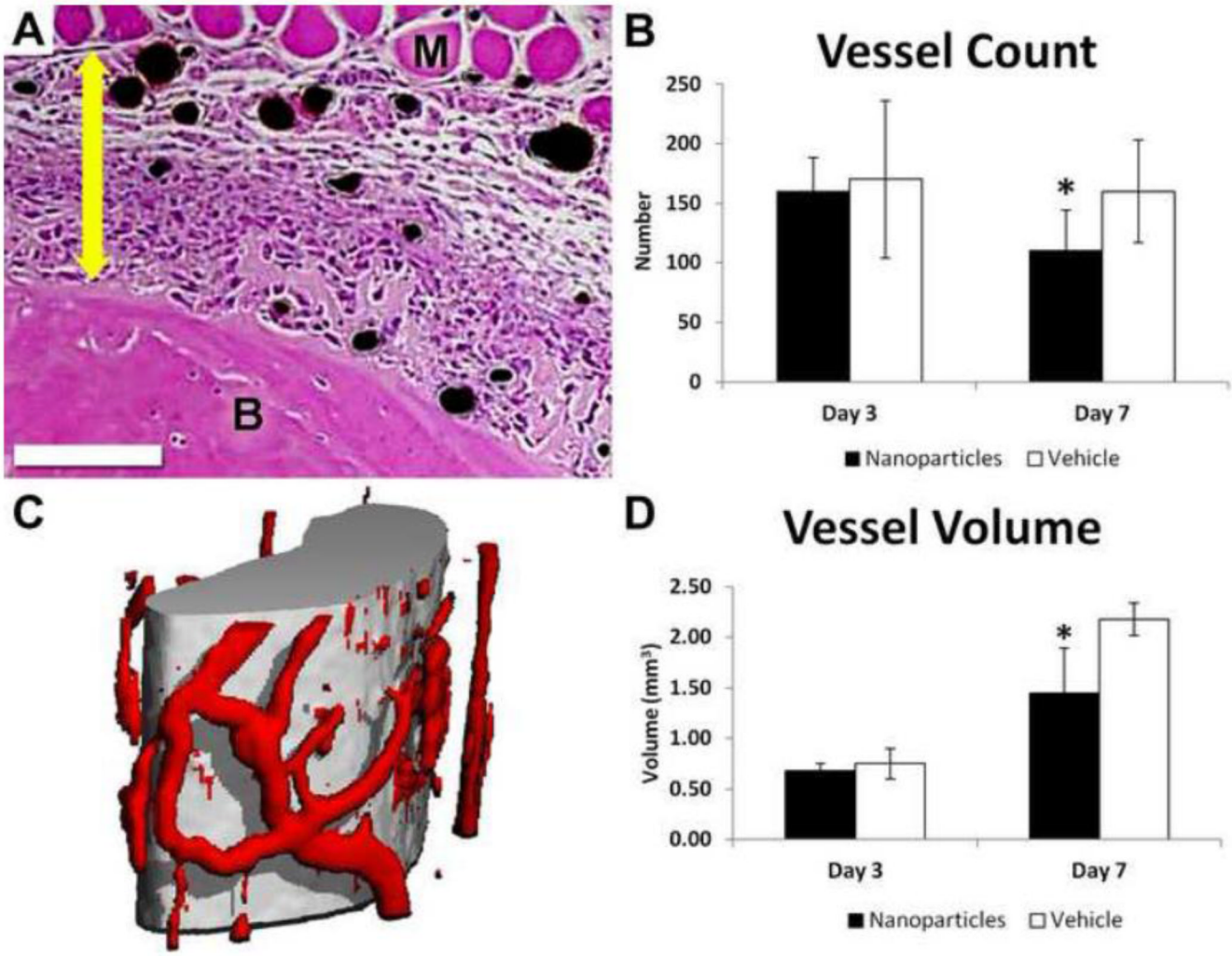

Fig. 3. Anti-angiogenic Treatment Reduced Vessel Count and Volume 7 days after Loading

(A) H&E stained cross-section of an ulna 3 days after loading, with bone labeled B, muscle labeled M, perfused vessels black, and the expanded periosteum marked with a double-headed arrow. Scale bar is 250 μm. (B) Quantification of vessel number in histological sections showed significantly fewer vessels in nanoparticle treated limbs (black) than vehicle (white) 7 days after loading. (C) MicroCT reconstruction of the midsection of the ulna (grey) with surrounding perfused vasculature (red). (D) Quantification of microCT images showed significantly less vessel volume in nanoparticle treated limbs (black) than vehicle (white) 7 days after loading. All values are mean ± standard deviation. * $p < 0.05$ vs. Vehicle.

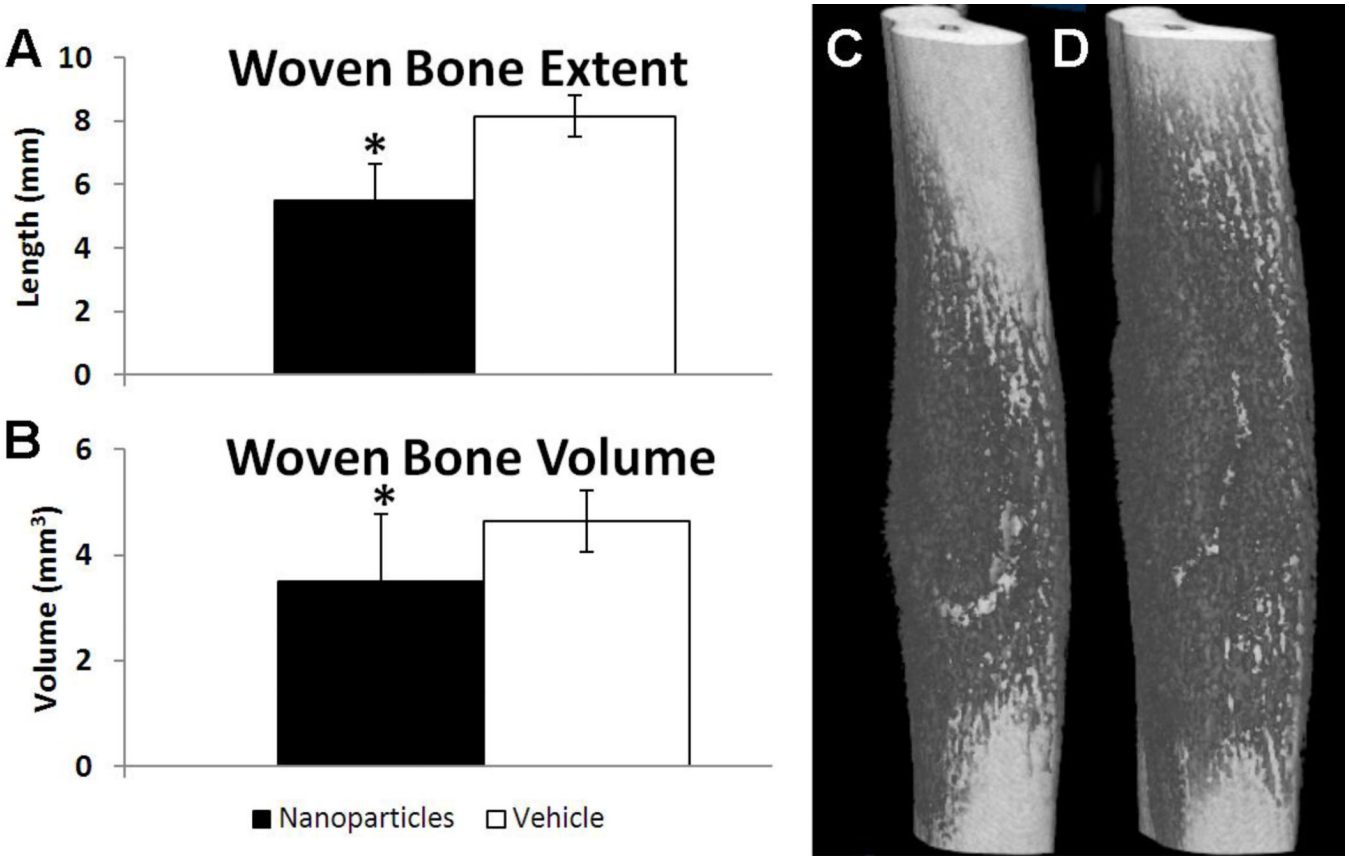

Fig. 4. Anti-angiogenic Treatment with Nanoparticles Impaired Woven Bone Formation 7 days after Loading

Woven bone formation after mechanical loading and treatment with nanoparticles (black) or vehicle (white) is given as mean ± standard deviation. Nanoparticle-treated limbs had significantly less woven bone formation as demonstrated by (A) woven bone extent and (B) woven bone volume measured by microCT. Representative microCT images of (C) nanoparticle and (D) vehicle treated ulnae illustrate differences in woven bone formation (dark grey). * $p < 0.05$ vs. Vehicle.

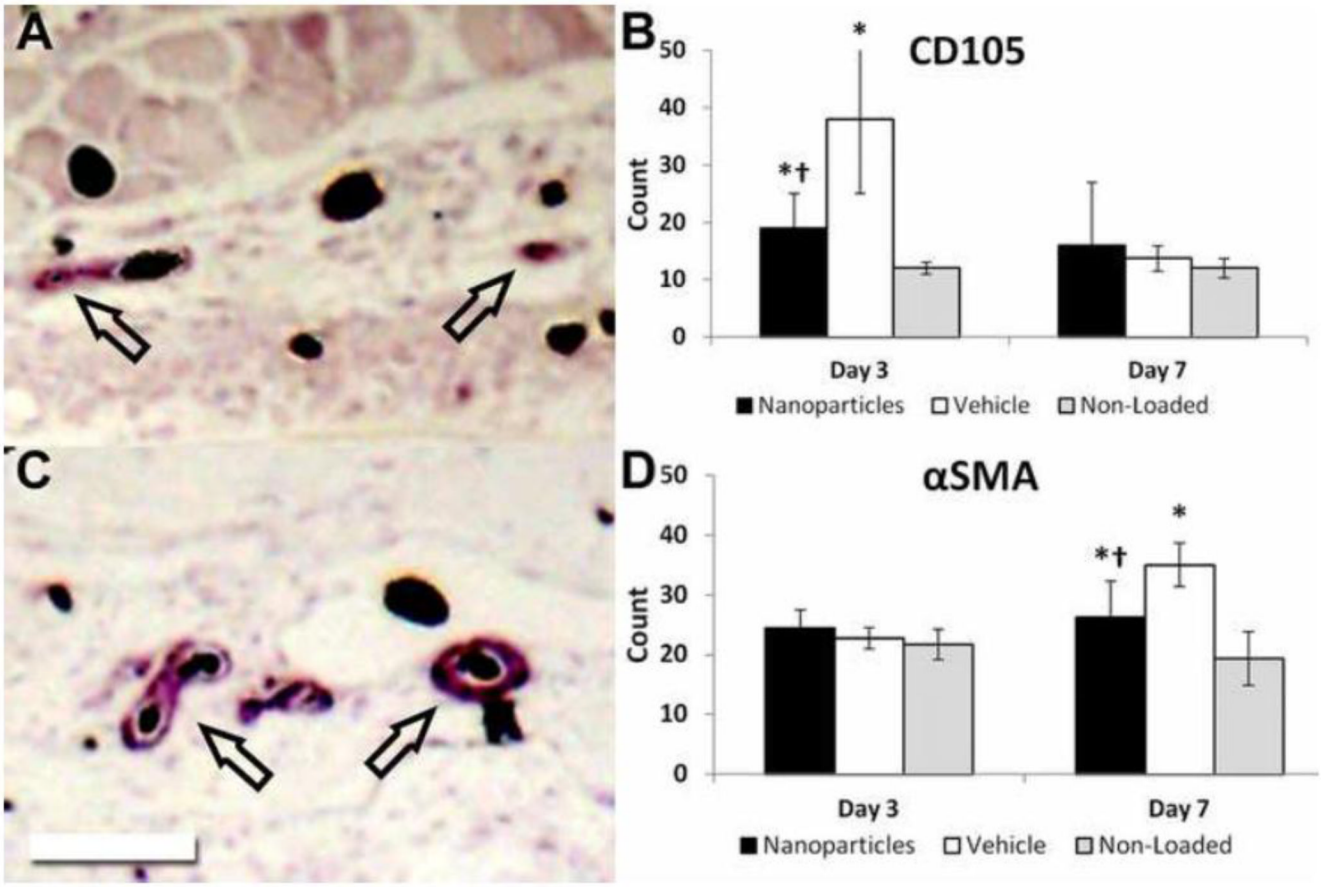

Fig. 5. Anti-Angiogenic Treatment Reduces the Early Increase in CD105 Positive Blood Vessels and the Later Increase in αSMA Positive Blood Vessels after Loading

Immunohistochemistry staining for (A) CD105 and (C) αSMA is quantified (B, D) for nanoparticle treated loaded limbs, vehicle treated loaded limbs, and non-loaded limbs. On day 3, treatment significantly reduced the number of CD105 positive blood vessels. By day 7, this resulted in a significant decrease in the number of αSMA positive blood vessels. Perfused vessels appear black, and arrows indicate positively stained vessels. Scale bar is 250 μm. *: $p < 0.05$ vs. Non-Loaded, †: $p < 0.05$ vs. Vehicle.